PNAS RESEARCH ARTICLE | DEVELOPMENTAL BIOLOGY OPEN ACCESS

TEX38 localizes ZDHHC19 to the plasma membrane and regulates sperm head morphogenesis in mice

Yuki Kaneda[a,b,1], Yonggang Lu[a,c,1,2], Jiang Sun[a,1], Keisuke Shimada[a], Chihiro Emori[a], Taichi Noda[a,d,e], Takayuki Koyano[f], Makoto Matsuyama[f], Haruhiko Miyata[a,2], and Masahito Ikawa[a,b,g,h,i,2]

Affiliations are included on p. 9.

Edited by Thomas Spencer, University of Missouri, Columbia, MO; received September 9, 2024; accepted January 22, 2025

Sperm morphogenesis is a tightly regulated differentiation process, disruption of which leads to sperm malfunction and male infertility. Here, we show that *Tex38* knockout (KO) male mice are infertile. *Tex38* KO spermatids exhibit excess retention of residual cytoplasm around the head, resulting in abnormal sperm morphology with backward head bending. TEX38 interacts and colocalizes with ZDHHC19, a testis-enriched acyltransferase catalyzing protein S-palmitoylation, at the plasma membrane of spermatids. ZDHHC19 and TEX38 are each downregulated in mouse testes lacking the other protein. TEX38 stabilizes and localizes ZDHHC19 to the plasma membrane of cultured cells and vice versa, consolidating their interdependence. Mice deficient in ZDHHC19 or harboring a C142S mutation that disables the palmitoyltransferase activity of ZDHHC19 display phenotypes resembling those of *Tex38* KO mice. Strikingly, ZDHHC19 palmitoylates ARRDC5, an arrestin family protein regulating sperm differentiation. Overall, our findings indicate that TEX38 forms a stable complex with ZDHHC19 at the plasma membrane of spermatids, which governs downstream S-palmitoylation of proteins essential for morphological transformation of spermatids.

S-acylation | spermiation | sterility

Significance

S-palmitoylation is a lipid posttranslational modification process involved in diverse cellular events in a wide range of biological systems. It has remained unclear whether S-palmitoylation has a role in male reproduction. Here, we found that TEX38 is important for the stability and plasma membrane localization of ZDHHC19, an S-palmitoylation enzyme, in the male germ cells. Ablation of TEX38 or disruption of the palmitoylation activity of ZDHHC19 in mice resulted in sperm head malformation and male infertility. This study demonstrates the essential role of S-palmitoylation in sperm head morphogenesis. A germline-specific, ZDHHC19-mediated posttranslational modification pathway sheds light on diagnosis of idiopathic male infertility and development of nonhormonal male contraceptives.

Mammalian spermatozoa are highly specialized cells composed of a head densely packed with the paternal genetic material and a flagellum regulating their motility. After mitotic and meiotic divisions, the male germ cells undergo spermiogenesis, during which they experience dramatic morphological changes including acrosome biogenesis, flagellar elongation, nuclear condensation, and mitochondrial rearrangement to transform into elongated spermatids (1). The fully differentiated spermatids are eventually released from the seminiferous epithelium to the lumen, in a process known as spermiation, and transported to the epididymis for further maturation (2, 3). Spermiation involves several discrete steps including remodeling of the spermatid head and cytoplasm, removal of specialized adhesion structures, and the final disengagement of the spermatids from Sertoli cells (3). During this process, the spermatid cytoplasm is separated from the spermatids and phagocytosed as a residual body by Sertoli cells (4). Abnormal morphogenesis of spermatozoa impairs their ability to fertilize oocytes and causes male infertility, which is a prevailing social issue that affects one in six couples of reproductive age (5). Although knockout (KO) studies in mice have identified genes essential for spermiogenesis over the past several decades (1, 6), the molecular mechanisms underlying this intricate process have not been fully elucidated.

S-acylation, or S-palmitoylation, is a reversible posttranslational modification of proteins, where long-chain fatty acids covalently attach to their cysteine residues. S-palmitoylation reportedly regulates membrane trafficking and modulates protein functions by increasing their hydrophobicity (7, 8). This process is mediated by the zinc finger Asp-His-His-Cys motif-containing (ZDHHC) family of protein acyltransferases (PATs), most of which are expressed in the endoplasmic reticulum (ER) and Golgi apparatus (9). Among the 23 known ZDHHCs, *Zdhhc11* and *Zdhhc19* are expressed predominantly in mouse testes. While *Zdhhc11* KO male mice are fertile, disruption of *Zdhhc19* results in male infertility with abnormal sperm head folding (10, 11). Distinct from other ZDHHC proteins, ZDHHC19 is localized to the plasma membrane of spermatids (10). However, it is unclear how its surface localization is regulated and whether the PAT activity of ZDHHC19 correlates with the KO phenotypes.

In this study, we disrupted TEX38, a transmembrane protein expressed predominantly in testes, in mice using the CRISPR/Cas9 system and found that *Tex38*$^{-/-}$ male mice are infertile with abnormal sperm head bending, which phenocopies *Zdhhc19*$^{-/-}$ mice. Further analyses revealed that TEX38 interacts with ZDHHC19; this interaction is essential for

Author contributions: Y.K., Y.L., H.M., and M.I. designed research; Y.K., Y.L., J.S., and K.S. performed research; Y.K., C.E., T.N., T.K., and M.M. contributed new reagents/analytic tools; Y.K., Y.L., J.S., and K.S. analyzed data; and Y.K., Y.L., H.M., and M.I. wrote the paper.

The authors declare no competing interest.

This article is a PNAS Direct Submission.

[1]Y.K., Y.L., and J.S. contributed equally to this work.

[2]To whom correspondence may be addressed. Email: lu.yonggang.prime@osaka-u.ac.jp, hmiya003@biken.osaka-u.ac.jp, or ikawa@biken.osaka-u.ac.jp.

This article contains supporting information online at https://www.pnas.org/lookup/suppl/doi:10.1073/pnas.2417943122/-/DCSupplemental.

Published March 3, 2025.

their stability and localization to the plasma membrane. Acyl-biotin exchange followed by proteomic analyses further uncovered that ZDHHC19 catalyzes S-palmitoylation of ARRDC5, disruption of which reportedly results in similar morphological anomalies in mouse spermatozoa (12, 13).

Results

TEX38 Is Necessary for Sperm Head Morphogenesis and Male Fertility. TEX38 contains an N-terminal hydrophobic region (the amino acid residues 4-26) predicted as a transmembrane domain by SMART (Fig. 1*A*). RT-PCR using cDNA from multiple mouse tissues revealed predominant expression of *Tex38* in testes (Fig. 1*B*). Further, *Tex38* expression was initially detected in the cDNA of postnatal day 21 mouse testes (Fig. 1*C*), which corresponds to the postmeiotic stage in the first wave of mouse spermatogenesis. To investigate the physiological role of *Tex38* in vivo, we established a *Tex38* KO mouse line (*Tex38*$^{-/-}$) using the CRISPR/Cas9 system (*SI Appendix*, Fig. S1*A*). Using two gRNAs flanking the coding region of *Tex38*, we introduced a deletion of 1,458 base pairs, confirmed by Sanger sequencing following genomic PCR (*SI Appendix*, Fig. S1 *A* and *B*). The KO mice showed no obvious abnormalities in development, appearance, or behavior. Nevertheless, despite successful copulation with wild-type (WT) females, *Tex38*$^{-/-}$ male mice did not sire any pups during the two-month mating period (Fig. 1*D*), suggesting that *Tex38* is indispensable for male fertility.

To examine the cause of male infertility in *Tex38*$^{-/-}$ mice, we performed morphological analyses of the male reproductive tract and spermatozoa. *Tex38*$^{-/-}$ mice showed normal testis weight (*SI Appendix*, Fig. S1*C*), but PAS staining of paraffin sections revealed that spermatids were retained in the seminiferous epithelium of stage VIII and IX tubules, while elongated spermatids were released in the tubules of the same stages in *Tex38*$^{+/-}$ mice (Fig. 1*E* and *SI Appendix*, Fig. S1*D*). Noticeably, round cells, presumably degenerated early spermatids, were detected in the cauda epididymides of *Tex38*$^{-/-}$ mice (Fig. 1*F*). Although no clear abnormalities were observed in the flagella of *Tex38* KO spermatozoa, their heads were abnormally folded backward (Fig. 1*G* and *SI Appendix*, Fig. S1*E*).

Several previous studies have reported a causal relationship between abnormal cytoplasmic droplet (CD) formation at sperm heads and sperm head bending (14–16). CD is a small piece of residual cytoplasm composed of saccular membranous structures derived from the ER and Golgi apparatus and widely conserved in vertebrate spermatozoa (17–19). After sperm releasing into the lumen of seminiferous tubules, their CDs migrate from the head to the flagellum (20). Immunofluorescence analyses showed strong signals of SYPL1, a CD marker (21), at the bent heads of *Tex38* KO spermatozoa, while SYPL1 was localized to the junction of the midpiece and principal piece in the control spermatozoa (Fig. 1*G*), suggesting that CDs are not formed correctly and excess residual cytoplasm remains in the KO sperm head. Transmission electron microscopy (TEM) further consolidated the irregular cytoplasm retention at the heads of *Tex38* KO spermatozoa (Fig. 1*H*). In addition, the sperm plasma membrane continuously extended from the bent head to the midpiece (red arrowheads) instead of invaginating at the bending site (Fig. 1*H*), implying a potential correlation between the excessive cytoplasmic space and instability of the head structure. Interestingly, folded spermatozoa were rarely observed in the KO testes, whereas spermatozoa with head folding were gradually increased during their transition from caput to corpus to cauda epididymides (Fig. 1 *I* and *J*), consistent with the timing of the CD movement from head to tail. These results collectively suggest that the impaired cytoplasm removal might cause the folding of *Tex38* KO spermatozoa.

We next examined the sperm motility by computer-assisted sperm analysis. The percentages of motile spermatozoa after 120 min incubation in a capacitating medium and progressively motile spermatozoa after 10 min and 120 min incubation were significantly lower in *Tex38*$^{-/-}$ males compared to the *Tex38*$^{+/-}$ control (*SI Appendix*, Fig. S1 *F* and *G*). In addition, sperm kinematics parameters, including average path velocity and straight line velocity, were significantly reduced in *Tex38* KO spermatozoa (*SI Appendix*, Fig. S1*H*).

Disruption of *Tex38* Leads to Defective Sperm Passage Through the UTJ. To further analyze the functionality of *Tex38* KO spermatozoa, we performed in vitro fertilization (IVF) using cumulus–oocyte complexes (cumulus-intact), oocytes without cumulus cells (cumulus-free), and oocytes without both cumulus cells and zona pellucida (ZP; ZP-free). As a result, *Tex38* KO spermatozoa failed to fertilize oocytes under all conditions (*SI Appendix*, Fig. S2 *A–C*), likely caused by the impaired sperm head morphology and motility. Further, we investigated whether *Tex38* KO spermatozoa can migrate through the uterotubal junction (UTJ) using *Tex38* KO Red Body Green Sperm (RBGS) transgenic (Tg) mice that express DsRed2 in mitochondria (22). While control spermatozoa could pass through the UTJ, *Tex38* KO spermatozoa were hardly found in the oviduct (*SI Appendix*, Fig. S2*D*). We then analyzed the processing of ADAM3, as well as the levels of ADAM3-related proteins tACE and PRSS37, by immunoblotting given the pivotal roles of these sperm head proteins in the UTJ migration (23, 24). ADAM3 and tACE were reduced, and PRSS37 was aberrantly retained in *Tex38* KO spermatozoa (*SI Appendix*, Fig. S2 *E* and *F*). The abnormal protein levels are likely a manifestation of altered sperm proteome derived from compromised cytoplasm removal and head shaping.

Next, we examined the possibility of rescuing the sterility of *Tex38* KO males by intracytoplasmic sperm injection (ICSI). We injected *Tex38* KO sperm heads into 71 oocytes and obtained 31 2-cell embryos. By transplanting these embryos into the oviducts of pseudopregnant females, we obtained two healthy pups harboring the KO allele (*SI Appendix*, Fig. S2 *G–I*), indicating that ablation of *Tex38* does not affect sperm DNA integrity or embryogenesis.

TEX38 Interacts with and Stabilizes ZDHHC19 and *Zdhhc19* KO Males Phenocopy *Tex38* KO Mice. To identify the interactome of TEX38 in mouse testes, we performed coimmunoprecipitation (co-IP) using an anti-TEX38 antibody and analyzed the precipitated protein complexes by mass spectrometry (MS; Dataset S1). We found ten proteins with more than five-fold decrease in *Tex38*$^{-/-}$ mice compared to the WT control (*SI Appendix*, Fig. S3*A*). These include microtubule affinity regulating kinase family proteins MARK1-4 and zinc finger DHHC-type containing 19 (ZDHHC19), a PAT catalyzing S-palmitoylation (9) (*SI Appendix*, Fig. S3*A*). While the protein levels of MARK1-4 were comparable between KO and control, the amount of ZDHHC19 was decreased in *Tex38*$^{-/-}$ testes (Fig. 2*A*). Intriguingly, a previous report has shown that the disruption of *Zdhhc19* results in folded sperm heads (10, 11), reminiscent of the phenotype of *Tex38*$^{-/-}$ mice. Therefore, we sought to reveal the molecular relationship between *Tex38* and *Zdhhc19*. According to previously published single-cell RNA-sequencing datasets, *Tex38* and *Zdhhc19* show peak expression in spermatids (Fig. 2*B*). Through co-IP and immunoblotting using testis lysates, we confirmed the interaction between TEX38 and ZDHHC19 (Fig. 2*C*).

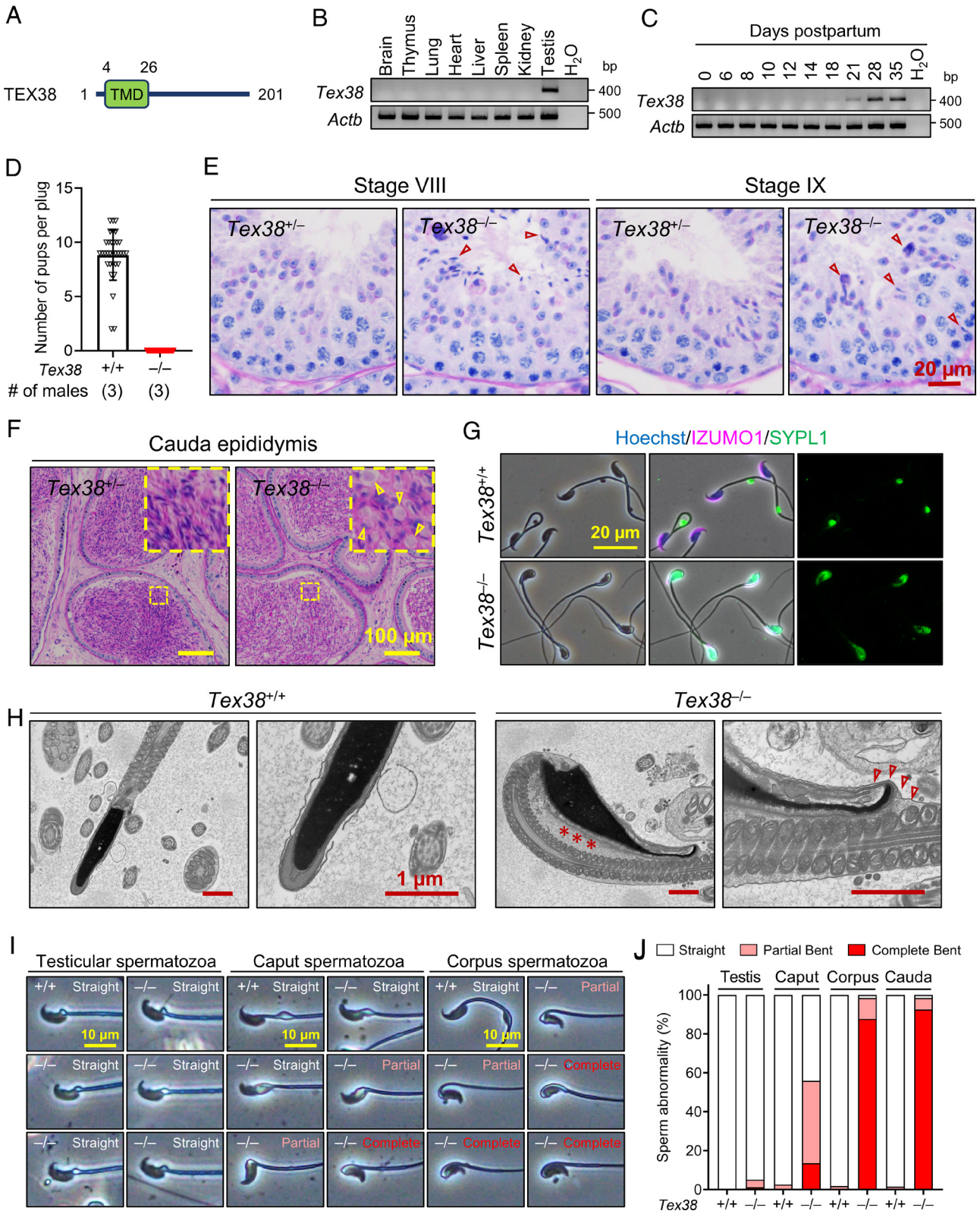

Fig. 1. *Tex38*$^{-/-}$ male mice were infertile due to sperm head folding. (*A*) A transmembrane domain (TMD) in TEX38 was predicted using SMART (http://smart.embl-heidelberg.de/). (*B*) RT-PCR of *Tex38* using RNAs of multiple adult mouse tissues. *Tex38* is predominantly expressed in the testis. *Actb* was used as a loading control. (*C*) RT-PCR of *Tex38* using RNAs obtained from postnatal day 0 to 35 mouse testes. (*D*) The numbers of pups per plug. WT or *Tex38*$^{-/-}$ male mice were individually mated with three WT females. (*E*) Histology of stage VIII and IX seminiferous tubules. Red arrowheads indicate unreleased sperm lining the lumen. (*F*) Histology of cauda epididymides. Yellow arrowheads indicate round cells, presumably degenerated early spermatids. (*G*) Immunostaining of IZUMO1 (magenta) and SYPL1 (green) in WT and *Tex38* KO spermatozoa. IZUMO1 and SYPL1 was used as a marker for the acrosome and CD, respectively. Nuclei were visualized with Hoechst 33342 (blue). (*H*) Ultrastructural analysis of cauda epididymal spermatozoa by TEM. Retained residual cytoplasm was observed in the sperm head (red asterisks). The sperm plasma membrane does not fold inward at the head bending site (red arrowheads). (*I*) Testicular and caput and corpus epididymal spermatozoa are subdivided into three morphological categories; straight (Straight), partially bent (Partial), and completely bent (Complete). (*J*) Percentages of spermatozoa with the three types of head abnormalities in WT and *Tex38*$^{-/-}$ male mice (n = 3). Head folding was rarely observed in testicular spermatozoa, while a multitude of folded spermatozoa appeared in the corpus and cauda epididymides.

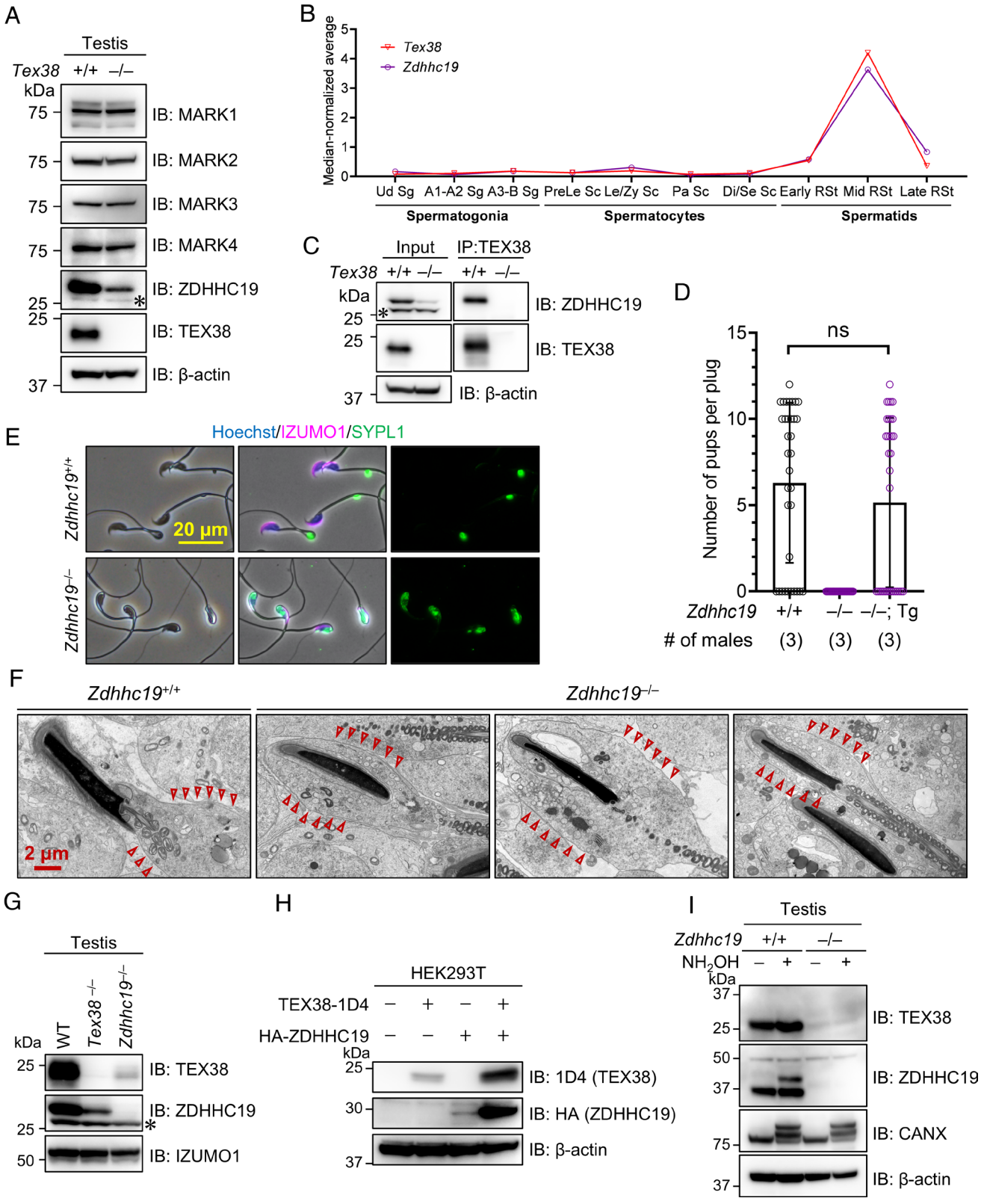

Fig. 2. TEX38 interacts with ZDHHC19, ablation of which phenocopies *Tex38*$^{-/-}$ male mice. (*A*) Immunoblot analyses of representative TEX38-interacting proteins identified by co-IP/MS in WT and *Tex38*$^{-/-}$ testes. β-actin was used as a loading control. The black asterisk indicates nonspecific bands. (*B*) Expression patterns of *Tex38* and *Zdhhc19* in mouse spermatogenic cells based on a previously published scRNA-seq dataset (25). (*C*) Validation of the interaction between TEX38 and ZDHHC19 in testes. ZDHHC19 was coimmunoprecipitated with TEX38. β-actin was used as a loading control. The black asterisk indicates nonspecific protein bands. (*D*) The numbers of pups per plug. (*E*) Immunostaining of IZUMO1 (magenta) and SYPL1 (green) in WT and *Zdhhc19* KO spermatozoa. IZUMO1 and SYPL1 was used as a marker for the acrosome and CD, respectively. Nuclei were visualized with Hoechst 33342 (blue). (*F*) Ultrastructural analysis of elongated spermatids by TEM. Red arrowheads indicate the cytoplasm of WT and *Zdhhc19* KO spermatids. (*G*) Immunoblot analyses of TEX38 and ZDHHC19 in WT, *Tex38*$^{-/-}$, and *Zdhhc19*$^{-/-}$ testes. IZUMO1 was used as a loading control. The black asterisk indicates nonspecific bands. (*H*) TEX38-1D4 and/or HA-ZDHHC19 were individually or simultaneously overexpressed in HEK293T cells. β-actin was used as a loading control. (*I*) acyl-MfTag exchange (AME) assay of proteins extracted from WT and *Zdhhc19*$^{-/-}$ testes. Palmitic acid was cleaved by NH_2OH and replaced by the MfTag. CANX was used as a positive control as it contains two S-palmitoylation sites. β-actin was used as a loading control.

To further analyze the relationship between TEX38 and ZDHHC19, we generated *Zdhhc19* KO mice using two gRNAs flanking the coding region of *Zdhhc19* (*SI Appendix*, Fig. S3*B*). A deletion of 10,075 base pairs was confirmed by Sanger sequencing following genomic PCR (*SI Appendix*, Fig. S3 *B* and *C*). Depletion of ZDHHC19 in KO testes and spermatozoa was confirmed by immunoblotting (*SI Appendix*, Fig. S3*D*). While no clear difference was observed in testis appearance or weight (*SI Appendix*, Fig. S3 *E* and *F*), *Zdhhc19*$^{-/-}$ male mice were infertile (10, 11), which was rescued by a transgene encoding N-terminally HA-tagged ZDHHC19 expressed in testes (Fig. 2*D* and *SI Appendix*, Fig. S3 *G* and *H*). *Zdhhc19* KO mice showed spermatozoa with folded heads (Fig. 2*E* and *SI Appendix*, Fig. S3*I*), incomplete removal of residual cytoplasm in the heads (Fig. 2*E*), sperm retention in the stage VIII seminiferous tubules (*SI Appendix*, Fig. S3*J*), round spermatid-like cells in the cauda epididymis (*SI Appendix*, Fig. S3*J*), impaired sperm motility (*SI Appendix*, Fig. S4 *A–C*), and sperm head folding during epididymal transit (*SI Appendix*, Fig. S4 *D–F*), resembling the phenotypes observed in *Tex38* KO males (Fig. 1 *D–J* and *SI Appendix*, Fig. S1 *D–H*). Furthermore, TEM analyses of testis ultrathin sections revealed that the residual cytoplasm was localized to the neck of step 15 to 16 spermatids in the control but was abnormally retained in the heads of *Zdhhc19* KO spermatids (Fig. 2*F* and *SI Appendix*, Fig. S4*G*), suggesting that defective cytoplasmic removal takes place during late spermiogenesis.

Using *Zdhhc19* KO RBGS Tg mice, we found that *Zdhhc19* KO spermatozoa hardly migrated through the UTJ (*SI Appendix*, Fig. S4*H*). The processing and/or abundance of ADAM3 and ADAM3-related proteins were also abnormal in *Zdhhc19*$^{-/-}$ mice (*SI Appendix*, Fig. S4 *I* and *J*). It is worth noting that ADAM1B, a sperm head surface protein not related to ADAM3 processing or sperm UTJ migration (26), remained partially unprocessed in *Zdhhc19* KO spermatozoa (*SI Appendix*, Fig. S4*J*). Further, BASIGIN, a membrane protein localized in sperm tails, was mislocalized to the heads of *Zdhhc19* KO spermatozoa (*SI Appendix*, Fig. S4*K*). Since abnormal levels are not restricted to ADAM3-related proteins, we anticipate that cytoplasmic retention and sperm head malformation alter the sperm proteome and compromise the sperm function.

ZDHHC19 Stabilizes and Colocalizes with TEX38 at the Plasma Membrane of Spermatids. ZDHHC19 was significantly downregulated in *Tex38*$^{-/-}$ testes; likewise, TEX38 was drastically decreased in *Zdhhc19*$^{-/-}$ testes (Fig. 2*G* and *SI Appendix*, Fig. S5*A*), suggesting an interdependent relationship between these two proteins. We individually or simultaneously expressed ZDHHC19 and TEX38 in HEK293T cells and found elevated levels of ZDHHC19 and TEX38 in coexpressed cells (Fig. 2*H* and *SI Appendix*, Fig. S5*B*), indicating that ZDHHC19 and TEX38 stabilize each other by forming a heterodimer. To analyze whether TEX38 is palmitoylated in testes, we performed an AME assay which replaces palmitic acid with a multifunctional tag (MfTag) to induce a detectable size increase of palmitoylated proteins. A band shift was observed in CANX, a positive control of palmitoylation (27); however, no band shift was observed in TEX38 (Fig. 2*I*), suggesting that TEX38 is not a substrate protein of ZDHHC19-mediated S-palmitoylation. It is worth noting that a single band shift was observed in ZDHHC19 itself (Fig. 2*I*), which may be autoacylation for transferring palmitic acid from ZDHHC19 to its substrates (28).

We predicted the structure of the TEX38–ZDHHC19 heterodimer by AlphaFold3 (Fig. 3*A* and *SI Appendix*, Fig. S6) (29). Transmembrane domains of TEX38 and ZDHHC19 are closely associated and the C-terminal region of TEX38 interacts with ZDHHC19 in the cytosol (Fig. 3*A* and *SI Appendix*, Fig. S6). To further understand the relationship between TEX38 and ZDHHC19, we examined their subcellular localization in testes by immunohistochemistry. TEX38 and ZDHHC19 were colocalized to the plasma membrane of round and elongating spermatids (Fig. 3*B* and *SI Appendix*, Figs. S7 and S8). Protein fractionation further revealed that TEX38 was enriched in the plasma membrane fraction of testes (Fig. 3*C*). In corroboration with the immunoblot analyses (Fig. 3*C*), ZDHHC19 and TEX38 were undetectable in the plasma membranes of *Tex38* and *Zdhhc19* KO spermatids (Fig. 3*B* and *SI Appendix*, Fig. S8). Instead, they were weakly detected near the proacrosome of KO spermatids (Fig. 3*B*), likely to be the Golgi apparatus. Remarkably, in Cos-7 cells, individually expressed TEX38 and ZDHHC19 were localized to the Golgi apparatus, whereas coexpressed proteins were both trafficked to the plasma membrane (Fig. 3*D* and *SI Appendix*, Fig. S9*A* and *B*). Overall, our results indicate that TEX38 complexes with ZDHHC19 to be translocated to the plasma membrane.

Protein S-Acyltransferase Activity of ZDHHC19 Is Crucial for Spermiogenesis. The transfer of palmitate moiety to substrates is catalyzed by ZDHHC enzymes and requires autoacylation of cysteine within the DHHC domain to form a palmitoylated intermediate (28). ZDHHC19 contains a DHHC domain between the second and third transmembrane domains (Fig. 4*A*). We predicted the complex of TEX38 and the autoacylation intermediate of ZDHHC19 by AlphaFold3 and did not detect a steric clash in their binding interface (Fig. 4*B* and *SI Appendix*, Fig. S10). To interrogate whether the PAT activity of ZDHCC19 facilitates male reproduction, we generated a *Zdhhc19* mutant mouse line carrying a C142S mutation that ablates autoacylation of the DHHC domain (Fig. 4*C*) (30). The C142S mutation was confirmed by Sanger sequencing (Fig. 4*D*). Despite that the amount of ZDHHC19 and ZDHHC19 C142S proteins were comparable in WT and *Zdhhc19* (C142S) KI testes (*SI Appendix*, Fig. S11*A*), the cauda epididymal spermatozoa of *Zdhhc19*$^{C142S/C142S}$ mice showed abnormal head folding (Fig. 4*E* and *SI Appendix*, Fig. S11*B*), consistent with *Zdhhc19* KO spermatozoa. These results suggest that the PAT activity of ZDHHC19 is important for sperm head morphogenesis.

To identify potential substrates of ZDHHC19 in testes, we performed co-IP using anti-ZDHHC19 antibody and analyzed the immunoprecipitated proteins by MS (Dataset S2). We found 130 proteins that showed different binding abilities to WT ZDHHC19 and C142S ZDHHC19 [FC (WT/C142S) > 3 or FC (C142S/WT) > 3] (Fig. 4*F*). To further narrow down the substrate candidates, we performed an ABE assay, which allows us to purify S-palmitoylated proteins by labeling palmitoylated cysteine residues with a biotin probe (32). Through subsequent MS analyses (Dataset S3), we found 79 proteins that were more S-palmitoylated in WT compared to *Zdhhc19*$^{-/-}$ testes [FC (WT/KO) > 3] (Fig. 4*F*). Remarkably, ARRDC5, PLA2G6, AP1M1, and RAI14 were detected in both the co-IP/MS and ABE/MS analyses (Fig. 4*G*). Among these four proteins (12, 13, 33–35), it has been reported that *Arrdc5* KO mice show abnormal sperm morphology with head folding (12, 13), similar to *Zdhhc19* and *Tex38* KO mice. Strikingly, ZDHHC19 interacted with ARRDC5 in HEK293T cells (*SI Appendix*, Fig. S11*C*) and AME assay revealed that ARRDC5 was palmitoylated when coexpressed with WT ZDHHC19 but not with the C142S mutant (Fig. 4*H*). Because ARRDC5 was palmitoylated weakly even without ZDHHC19 likely due to the endogenous ZDHHCs in HEK293T cells, we performed the same assay using COS-7 cells and

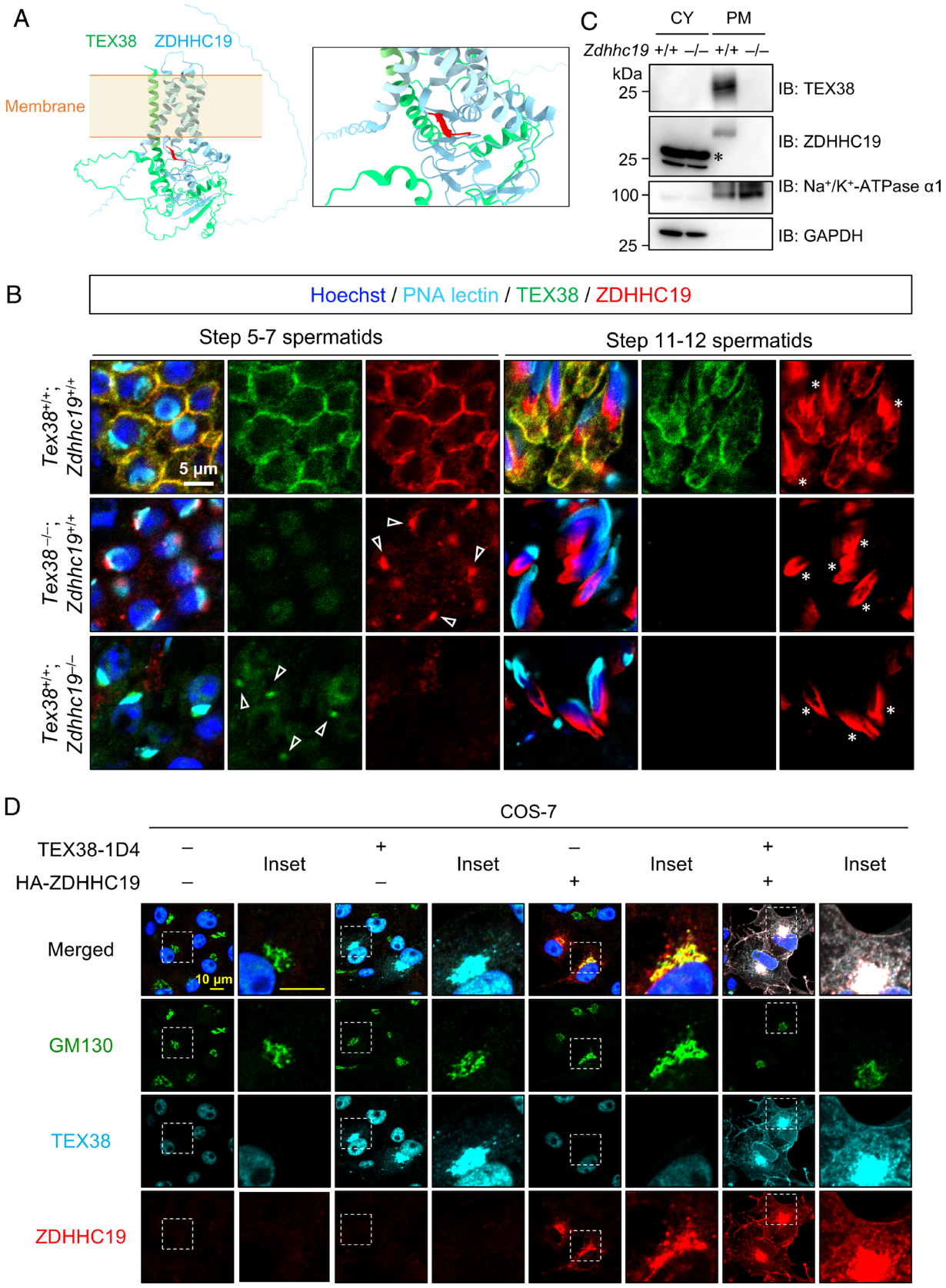

Fig. 3. TEX38 and ZDHHC19 colocalize at the plasma membrane of spermatids. (*A*) The structure of the TEX38–ZDHHC19 heterodimer predicted by AlphaFold3. The DHHC domain of ZDHHC19 is colored in red. (*B*) Immunostaining of TEX38 and ZDHHC19 in testis cryosections. TEX38 and ZDHHC19 were localized to the plasma membrane of WT spermatids and to the Golgi apparatus (white arrowheads) near the proacrosome of the KO spermatids lacking the other protein. The nuclei and acrosome of spermatids were visualized with Hoechst 33342 (blue) and lectin-PNA (cyan), respectively. White asterisks indicate nonspecific signals observed in the manchette. (*C*) Fractionation analyses of testis proteins. CY and PM indicate cytosol and plasma membrane, respectively. Na^+/K^+-ATPase α1 was used as a positive control for the plasma membrane fraction while GAPDH was used as a positive control for the cytosol fraction. The black asterisk indicates nonspecific bands. (*D*) TEX38-1D4 and/or HA-ZDHHC19 were individually or simultaneously expressed in COS-7 cells for immunocytochemistry analyses. The nuclei and Golgi apparatus of COS-7 cells were visualized with Hoechst 33342 (blue) and an anti-GM130 antibody (Green), respectively.

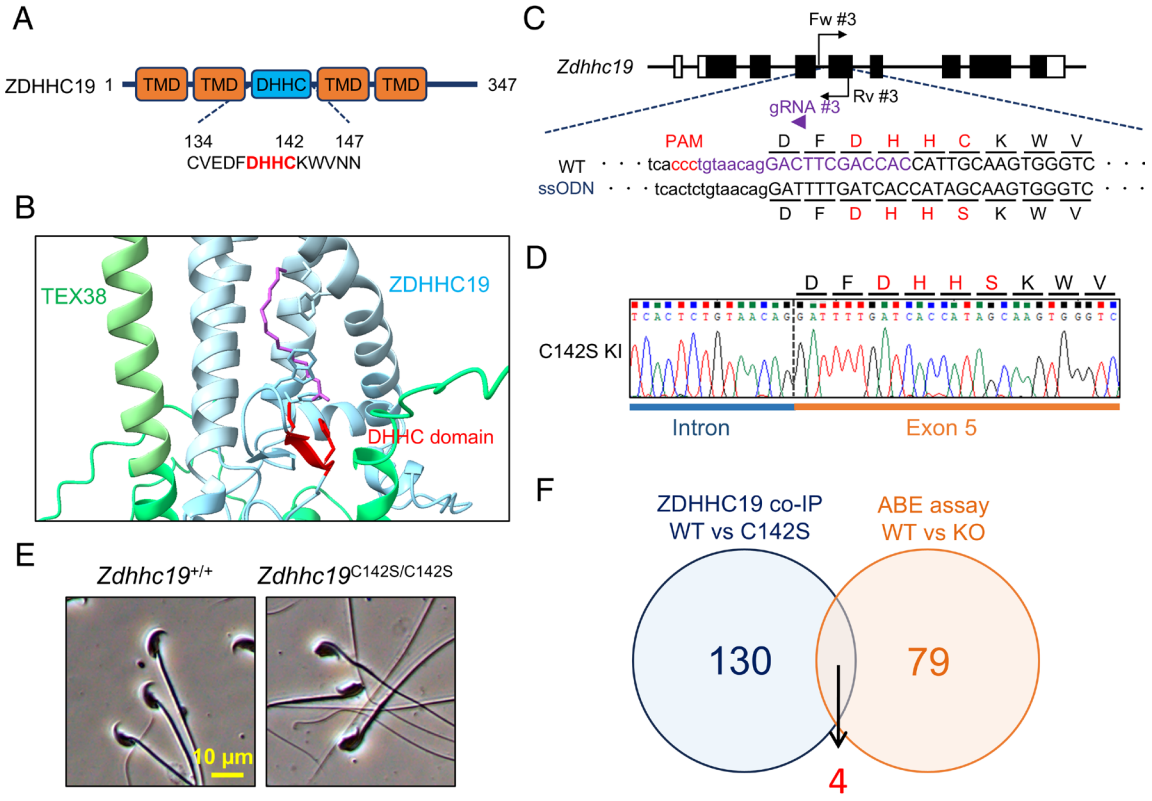

G

Accession	Proteins	Peptides detected by IP-MS		Palmitoylation score by ABE		Testis palmitoyl-proteome (31)	Fertility of null mice
		Zdhhc19$^{+/+}$	*Zdhhc19*$^{CS/CS}$	*Zdhhc19*$^{+/+}$	*Zdhhc19*$^{-/-}$		
Q497K5	ARRDC5	6.2	0.1	22.9	1.0	Detected	Sterile (12,13)
P97819	PLA2G6	4.1	1.1	1.3	0.4	Detected	Severe infertile (33)
P35585	AP1M1	0.1	2.1	2.3	0.1	Detected	Embryonic lethal (34)
Q9EP71	RAI14	1.1	4.1	0.7	0.2	Detected	Fertile (35)
A2A8T7	TEX38	64.6	48.5	Undetected	Undetected	Undetected	Sterile
B9EIU6	ZDHHC19	49.5	30.7	Undetected	Undetected	Detected	Sterile

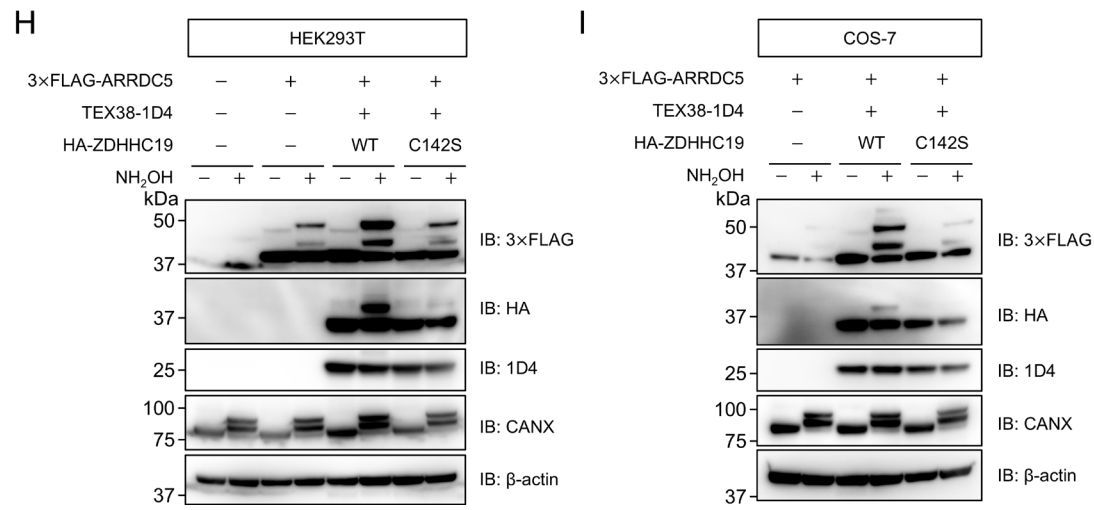

Fig. 4. The PAT activity of ZDHHC19 is important for sperm head morphogenesis. (*A*) The domain composition of ZDHHC19. Cysteine 142 in the DHHC domain is crucial for autoacylation. TMD indicates a transmembrane domain. (*B*) The complex of TEX38 and the autoacylated ZDHHC19 predicted by AlphaFold3. The DHHC domain of ZDHHC19 was colored in red. Palmitic acid is indicated in purple. (*C*) Schematics of generating *Zdhhc19*$^{C142S/C142S}$ mice by CRISPR/Cas9. White and black boxes indicate untranslated regions and protein coding regions, respectively. gRNAs are shown in purple. (*D*) Confirmation of the C142S KI mutation with direct sequencing of the PCR product amplified by Fw #3 and Rv #3 primers. (*E*) Morphology of spermatozoa obtained from the cauda epididymides of WT and *Zdhhc19*$^{C142S/C142S}$ mice. (*F*) Proteomic analyses unraveling potential substrates of ZDHHC19 in testes. Co-IP/MS analyses detected 130 proteins showing differential binding ability to WT and C142S mutant ZDHHC19 [FC (WT/C142S) > 3 = 82 proteins; FC (C142S/WT) > 3 = 48 proteins]. acyl-biotin exchange (ABE)/MS analyses detected 79 proteins that were higher palmitoylated in WT than *Zdhhc19*$^{-/-}$ testes [FC (WT/KO) > 3]. (*G*) Four top hits of ZDHHC19 substrates detected in both co-IP/MS and ABE/MS. All four proteins were previously identified as candidate palmitoylated proteins in testes (31). (*H*) AME assay of ZDHHC19-mediated palmitoylation in HEK293T cells. (*I*) AME assay of ZDHHC19-mediated palmitoylation in COS-7 cells.

confirmed that ARRDC5 was palmitoylated by WT but not the C142S mutant ZDHHC19 (Fig. 4*I*). It should be noted that the C142S mutant of ZDHHC19 itself was not palmitoylated, indicating that autoacylation occurs at the cysteine residue 142.

Discussion

During spermiogenesis, spermatids undergo drastic morphological changes, such as acrosome and flagellum formation, chromatin remodeling, and cytoplasmic elimination, which are essential for their fertilizing ability. Several KO mice have been reported to show defective spermiogenesis and male infertility with sperm head folding (12–16). Here, we found that *Tex38* is necessary for male fertility in mice; *Tex38*$^{-/-}$ mice showed impaired spermiation and abnormal sperm head bending. Further, *Tex38* KO spermatozoa could hardly migrate through the UTJ, which may be the primary cause of male infertility.

We demonstrated that TEX38 interacts with ZDHHC19, disruption of which results in similar phenotypes to those of *Tex38*$^{-/-}$ mice. In both *Tex38*$^{-/-}$ and *Zddhc19*$^{-/-}$ mice, head folding is initially observed in the caput epididymal spermatozoa, which might originate from abnormal retention of residual cytoplasm in the heads of spermatids (Fig. 2*F* and *SI Appendix*, Fig. S4*G*). It has been reported that TSKS-disrupted male mice are infertile with spermiation defects (36). The absence of TSKS induces excess residual cytoplasm due to abnormal cytoplasmic elimination by Sertoli cells, which causes apoptosis in KO epididymal spermatozoa, but there are no overt abnormalities in cytoplasmic elimination around the nucleus. On the other hand, mice lacking SPEM1, a testis-enriched cytoplasmic protein, show sperm head folding likely due to retained cytoplasmic components in the sperm head and neck, which may mechanically prevent sperm heads from stretching straight (16). Similarly, our ultrastructural analysis showed cytoplasmic elimination failure around the nucleus in *Zdhhc19*$^{-/-}$ mice, which may be the cause of abnormal head folding.

Recent studies have discovered that several ZDHHC enzymes require accessory proteins for their activity, stability, and localization (37). For instance, GCP16, a transmembrane protein localized to the Golgi apparatus, enhances the PAT activity and stability of ZDHHC9 (38). It has been shown that *Zdhhc19* is important for male fertility (10, 11), but the regulator of ZDHHC19 and its palmitoylated substrates during spermatogenesis were unknown. We demonstrated that TEX38 is necessary for the stability and plasma membrane localization of ZDHHC19 independent of S-palmitoylation in testes. Our TEX38 co-IP/MS analyses also uncovered the interactions between TEX38 and MARK1-4. These MARK family proteins are also candidate interactome of ZDHHC19 detected by co-IP/MS (Dataset S2). MARKs are kinases underpinning microtubule stability by phosphorylating microtubule-associated proteins such as tau, MAP2, and MAP4 (39). Previous studies have revealed that MARK family proteins are involved in a variety of cellular events such as cell polarity (40, 41), cell cycles, mitotic spindle regulation (42, 43), and cell migration (44–46). Among MARK family proteins, MARK2 and MARK4 are predominantly expressed in testes (47). Intriguingly, disruption of MARK2 in mice causes male subfertility with no obvious sperm morphological abnormalities (48) and MARK4 is dispensable for male fertility in mice (49) despite its implications in spermiation in rat testes (50). It has been shown that MARK2 and MARK3 can compensate for each other (51), suggesting that single gene KO of MARK family proteins may not exhibit clear phenotypes. Although our ABE/MS and previously published palmitoyl proteomics (31) did not identify S-palmitoylation in MARK family proteins, it is still possible that MARK family proteins collaborate with the TEX38-ZDHHC19 heterodimer to orchestrate sperm head morphogenesis. It is worth noting that our anti-ZDHHC19 antibody nonspecifically binds sperm manchette (Fig. 3*B*), a microtubule-based transient structure, potentially complicating the interpretation of the MS outcomes. Future investigations are warranted to determine whether or not ZDHHC19 has direct interactions with cytoskeletal proteins in the male germ cells.

Combining co-IP/MS and ABE/MS, we have identified four proteins including ARRDC5 as promising substrates of ZDHHC19. Our in vitro studies uncovered that ZDHHC19 palmitoylates ARRDC5, which belongs to the α-arrestin family involved in the endocytosis of membrane proteins (52). ARRDC5 may be palmitoylated by ZDHHC19 at two cysteine residues, given the two higher molecular weight bands detected in our AME assay (Fig. 4 *H* and *I*). Among the α-arrestin family proteins, ARRDC5 is unique in that it lacks a PPxY motif necessary for the interaction with E3 ubiquitin ligases (53) and is expressed predominantly in testes (12, 13). Recent studies have shown that disruption of *Arrdc5* in mice results in abnormal sperm morphology and male infertility (12, 13), which resembles the phenotypes observed in *Tex38*$^{-/-}$ and *Zdhhc19*$^{-/-}$ mice. Liu et al. discovered that NDC1 and SUN5, which are crucial components of the head–tail coupling apparatus (54, 55), are decreased in *Arrdc5* KO spermatozoa and ARRDC5 regulates the localization of NDC1 and SUN5 through SEC22A-mediated membrane trafficking (13). In addition, proteomics analyses indicated that ARRDC5 is enriched in mouse CDs (19). Combining these previous works and our present discoveries, we propose that ablation of ZDHHC19 disrupts ARRDC5-mediated membrane trafficking, thereby impairing cytoplasmic removal, CD formation, and sperm head shaping.

In this study, we found that TEX38 forms a stable heterodimer with ZDHHC19 at the plasma membrane of spermatids and the PAT activity of ZDHHC19 is important for correct sperm head shaping. Since TEX38 and ZDHHC19 are both conserved in humans, a germline-specific, ZDHHC19-mediated posttranslational modification pathway may contribute to understanding the etiology of infertility in men and developing nonhormonal male contraceptives that perturb the interaction between TEX38 and ZDHHC19 or the PAT activity of ZDHHC19.

Materials and Methods

Generation of *Tex38* KO and *Zdhhc19* KO, KI, and Tg Mouse Lines. *Tex38*$^{-/-}$ and *Zdhhc19*$^{-/-}$ mice were generated using the CRIPSR/Cas9 system as previously described (56). Briefly, two guide RNAs (gRNAs) were designed to remove the coding region largely. The CRISPR/Cas9 complexes were introduced into the 2PN embryos obtained from superovulated B6D2F1 females mated with B6D2F1 males using the super electroporator NEPA21 (NEPA GENE, Chiba, Japan). The electroporated embryos were cultured in KSOM medium (57) until the two-cell stage and transplanted into the oviducts of day 0.5 pseudopregnant ICR females. Founder mice obtained from natural delivery or Caesarean section were genotyped by PCR using forward (Fw) and reverse (Rv) primers and the deleted sequence was subsequently confirmed by Sanger sequencing.

Zdhhc19$^{C142S/C142S}$ KI mice were generated similarly by CRIPSR/Cas9. A gRNA was designed to target the DHHC domain of ZDHHC19 and a 128 bp long single-stranded oligonucleotide (ssODN) was used to mutate the cysteine of the DHHC domain to serine and to introduce additional synonymous mutations to avoid reediting of the KI site. The ssODN and the CRISPR/Cas9 complex were electroporated into B6D2 zygotes. The embryos were then cultured overnight and transplanted into pseudopregnant females. Founder mice were genotyped by sequencing the PCR amplicon of the KI region.

For generating *HA-Zdhhc19* Tg mice, N-terminally human influenza hemagglutinin (HA)-tagged *Zdhhc19* was inserted into the plasmid containing a *Clgn* promoter and a rabbit beta globin polyadenylation (polyA) signal (Addgene, Plasmid #173686). The linearized plasmid was microinjected into the pronuclei of

Zhddc19 heterozygous or homozygous KO embryos obtained by IVF. The injected embryos were cultured overnight and transplanted into the pseudopregnant females. Transgene was confirmed by PCR using primers targeting the N-terminal ORF and the polyA signal. Sequences of primers, gRNAs, and ssODN are listed in *SI Appendix*, Table S1.

Assessment of Male Fertility. For in vivo fertility tests, sexually mature KO or KO;Tg male mice were caged with three two-month-old B6D2F1 female mice, and vagina plugs were checked every morning and the number of pups were counted at birth. After the 8-wk mating period, the male mice were withdrawn from the cages, and the females were allowed to deliver their final litters. The IVF tests were performed as previously described (56) with minor changes–ZP-free oocytes were inseminated at a density of 2×10^4 spermatozoa per mL. ICSI was performed as previously described (56).

Observation of Sperm Migration Inside the Female Reproductive Tract. Sperm migration along the female reproductive tract was observed as previously described (56). *Tex38*$^{-/-}$ or *Zdhhc19*$^{-/-}$ mice were crossed with Tg mice expressing CAG/Su9-DsRed2, Acr3-EGFP (RBGS) (22). Sexually mature B6D2F1 females were superovulated and mated with RBGS male mice. Female mice were euthanized according to the approved procedure by the Osaka University Institutional Animal Care and Use Committee 4 h after confirming the formation of a vaginal plug. The female tract, from uterus to oviduct, were collected and examined under a BZ-X710 microscope (Keyence, Osaka, Japan).

Immunoprecipitation. Immunoprecipitation (IP) was performed as described previously (58). Testes or cultured cells were lysed in 1% Triton X-100 lysis buffer [1% Triton X-100, 50 mM Tris-HCl pH 7.4, 150 mM NaCl, 1% (v/v) phosphatase inhibitor cocktail (Nacalai Tesque, Kyoto, Japan), 1% (v/v) protease inhibitor cocktail (Nacalai Tesque)] at 4 °C with end-over-end rotation for 1 h. After centrifugation of lysates at 15,300×*g* for 15 min at 4 °C, the supernatants were collected. For TEX38 co-IP analyses, immune complexes were eluted with 2 × SDS sample buffer (132 mM Tris HCl pH 6.8, 4% SDS, 20% glycerol, and 0.01% Bromophenol Blue) for 10 min at 70 °C and used for subsequent immunoblotting or MS. For ZDHHC19 co-IP/MS analyses, precipitated protein complexes were eluted by on-beads trypsin digestion. LC–MS/MS was performed by the BIKEN MS core at Osaka University, Japan. Antibodies used for co-IP are listed in *SI Appendix*, Table S2. For determining the fold changes, 0.1 was added to each spectral count value to avoid division by zero.

Immunostaining of Testis Cryosections, Spermatozoa, and Cultured Cells. Immunostaining of testis cross-sections, spermatozoa, and COS-7 cells (#RCB0539, RIKEN BioResource Research Center) were performed as previously described (56). For immunostaining of COS-7 cells, cells were reseeded on glass coverslips 18 h after transfection. To induce cell cycle synchronization, cells were cultured in a serum reduced medium [0.1% fetal bovine serum (Sigma-Aldrich, St. Louis, MO) in Dulbecco's Modified Eagle Medium] 20 h prior to fixation. Antibodies used for immunostaining are listed in *SI Appendix*, Table S2.

AME Assay. Protein palmitoylation was detected using Protein S-Palmitoylation Detection Kit (RapidsPALM, BioDynaics Laboratory Inc., Japan) according to the manufacturer's protocol. For assays using cultured cells, cells were harvested 24 h after transfection with expression vectors. Protein samples were divided into two groups, a noncleavage group (negative control) where MfTag-labeling was performed in the absence of hydroxylamine and a cleavage group in which MfTag-labeling was carried out with hydroxylamine.

ABE Assay. ABE assay was performed as previously described (32). Proteins were extracted from mouse testes using 4% SDS buffer [4% (w/v) SDS, 50 mM Tris, 5 mM EDTA, pH 7.4, and 1% (v/v) protease inhibitor cocktail (Nacalai Tesque)]. Then, 200 μg of testis proteins were subjected to ABE, followed by LC–MS/MS carried out in the BIKEN MS core. Palmitoylation score was calculated as + hydroxylamine)/− hydroxylamine ratio. For calculating the fold changes, 0.1 was added to each spectral count value to avoid division by zero.

Statistical Analysis. All statistical analyses in this study were performed using the two-tailed Welch's *t* test using Microsoft Office Excel 2016 (Microsoft Corporation, Redmond, WA). Differences were considered significant at $P < 0.05$ (*), $P < 0.01$ (**), $P < 0.001$ (***). Error bars represent SD.

Additional experimental procedures are provided in *SI Appendix*, Materials and Methods.

Data, Materials, and Software Availability. All study data are included in the article and/or supporting information.

ACKNOWLEDGMENTS. We would like to thank the members of both the Department of Experimental Genome Research and the Nonprofit Organization for Biotechnology Research and Development (Osaka University) for experimental assistance and discussion. We also thank the members of Core Instrumentation Facility, especially Ms. Keiko Murata for Sanger sequencing, Dr. Akinori Ninomiya and Dr. Fuminori Sugihara for MS analyses, and Ms. Hiroko Omori for ultrastructural analysis (Osaka University). Finally, we thank Dr. Shaogeng Tang (Yale University) for contributing valuable reagents. This research was supported by Japan Society for the Promotion of Science KAKENHI grants (JP23KJ1523 to Y.K., JP24K02033 to Y.L., JP23K05831 to K.S., JP24K09314 to C.E., JP22H03214, JP23K18328 to H.M., and JP19H05750, JP23K20043, JP21H05033 to M.I.); Takeda Science Foundation grant to Y.L., K.S., T.N., H.M., and M.I.; JST FOREST (JPMJFR211F to H.M.); the Eunice Kennedy Shriver National Institute of Child Health and Human Development (P01HD087157 and R01HD088412 to M.I.); and the Bill & Melinda Gates Foundation (Grand Challenges Explorations grant INV-001902 to M.I.).

Author affiliations: [a]Department of Experimental Genome Research, Research Institute for Microbial Diseases, Osaka University, Suita, Osaka 5650871, JAPAN; [b]Laboratory of Experimental Genome Research, Graduate School of Pharmaceutical Sciences, Osaka University, Suita, Osaka 5650871, JAPAN; [c]Advanced Metrology Group, Premium Research Institute for Human Metaverse Medicine (WPI-PRIMe), Osaka University, Suita, Osaka 5650871, JAPAN; [d]Division of Reproductive Biology, Institute of Resource Development and Analysis, Kumamoto University, Kumamoto 8600811, JAPAN; [e]Priority Organization for Innovation and Excellence, Kumamoto University, Kumamoto 8608555, JAPAN; [f]Division of Molecular Genetics, Shigei Medical Research Institute, Okayama 7010202, JAPAN; [g]Laboratory of Reproductive Systems Biology, The Institute of Medical Science, The University of Tokyo, Minato-ku, Tokyo 1088639, JAPAN; [h]Division of Microbiology and Immunology, Center for Infectious Disease Education and Research (CiDER), Osaka University, Suita, Osaka 5650871, JAPAN; and [i]Team of Vaccine Evaluation, Center for Advanced Modalities and DDS (CAMaD), Osaka University, Suita, Osaka 5650871, JAPAN

1. H. Miyata, K. Shimada, Y. Kaneda, M. Ikawa, Development of functional spermatozoa in mammalian spermiogenesis. *Development* **151**, dev202838 (2024).
2. Y. Clermont, Kinetics of spermatogenesis in mammals: Seminiferous epithelium cycle and spermatogonial renewal. *Physiol. Rev.* **52**, 198–236 (1972).
3. L. O'Donnell, P. K. Nicholls, M. K. O'Bryan, R. I. McLachlan, P. G. Stanton, Spermiation. *Spermatogenesis* **1**, 14–35 (2011).
4. H. Breucker, E. Schäfer, A.-F. Holstein, Morphogenesis and fate of the residual body in human spermiogenesis. *Cell Tissue Res.* **240**, 303–309 (1985).
5. A. Agarwal, A. Majzoub, N. Parekh, R. Henkel, A schematic overview of the current status of male infertility practice. *World J. Men's Health* **37**, 308–322 (2019).
6. W. Yan, Male infertility caused by spermiogenic defects: Lessons from gene knockouts. *Mol. Cell Endocrinol.* **306**, 24–32 (2009).
7. Y. Fukata, M. Fukata, Protein palmitoylation in neuronal development and synaptic plasticity. *Nat. Rev. Neurosci.* **11**, 161–175 (2010).
8. M. E. Linder, R. J. Deschenes, Palmitoylation: Policing protein stability and traffic. *Nat. Rev. Mol. Cell Biol.* **8**, 74–84 (2007).
9. P. Ko, S. J. Dixon, Protein palmitoylation and cancer. *EMBO Rep.* **19**, e46666 (2018).
10. Y. Wu *et al.*, ZDHHC19 localizes to the cell membrane of spermatids and is involved in spermatogenesis. *Biol. Reprod* **106**, 477–486 (2022).
11. S. Wang, H. Qiao, P. Wang, Y. Wang, D. Qin, ZDHHC19 is dispensable for spermatogenesis, but is essential for sperm functions in mice. *Int. J. Mol. Sci.* **22**, 8894 (2021).
12. M. I. Giassetti *et al.*, ARRDC5 expression is conserved in mammalian testes and required for normal sperm morphogenesis. *Nat. Commun.* **14**, 2111 (2023).
13. R. Liu *et al.*, ARRDC5 deficiency impairs spermatogenesis by affecting SUN5 and NDC1. *Development* **150**, dev201959 (2023).
14. X. Zhang *et al.*, DDB1- and CUL4-associated factor 8 plays a critical role in spermatogenesis. *Front Med.* **15**, 302–312 (2021).
15. C. Li *et al.*, Spem2, a novel testis-enriched gene, is required for spermiogenesis and fertilization in mice. *Cellular Mol. Life Sci.* **81**, 108 (2024).
16. H. Zheng *et al.*, Lack of Spem1 causes aberrant cytoplasm removal, sperm deformation, and male infertility. *Proc. Natl. Acad. Sci. U.S.A.* **104**, 6852–6857 (2007).
17. R. Oko, L. Hermo, P. T. Chan, A. Fazel, J. J. Bergeron, The cytoplasmic droplet of rat epididymal spermatozoa contains saccular elements with Golgi characteristics. *J. Cell Biol.* **123**, 809–821 (1993).
18. G. Bloom, L. Nicander, On the ultrastructure and development of the protoplasmic droplet of spermatozoa. *Zeitschrift für Zellforschung und Mikroskopische Anatomie* **55**, 833–844 (1961).
19. S. Yuan, H. Zheng, Z. Zheng, W. Yan, Proteomic analyses reveal a role of cytoplasmic droplets as an energy source during epididymal sperm maturation. *PLoS ONE* **8**, e77466 (2013).

20. L. Hermo, R. -Marc Pelletier, D. G. Cyr, C. E. Smith, Surfing the wave, cycle, life history, and genes/proteins expressed by testicular germ cells. Part 3: Developmental changes in spermatid flagellum and cytoplasmic droplet and interaction of sperm with the zona pellucida and egg plasma membrane. *Microsc Res. Tech* **73**, 320–363 (2010).
21. J. Liu *et al.*, SYPL1 defines a vesicular pathway essential for sperm cytoplasmic droplet formation and male fertility. *Nat. Commun.* **14**, 5113 (2023).
22. H. Hasuwa *et al.*, Transgenic mouse sperm that have green acrosome and red mitochondria allow visualization of sperm and their acrosome reaction in vivo. *Exp. Anim.* **59**, 105–107 (2010).
23. Y. Fujihara *et al.*, Identification of multiple male reproductive tract-specific proteins that regulate sperm migration through the oviduct in mice. *Proc. Natl. Acad. Sci. U.S.A.* **116**, 18498–18506 (2019).
24. R. Yamaguchi, K. Yamagata, M. Ikawa, S. B. Moss, M. Okabe, Aberrant distribution of ADAM3 in sperm from both angiotensin-converting enzyme (Ace)- and calmegin (Clgn)-deficient mice. *Biol. Reprod.* **75**, 760–766 (2006).
25. B. P. Hermann *et al.*, The mammalian spermatogenesis single-cell transcriptome, from spermatogonial stem cells to spermatids. *Cell Rep.* **25**, 1650–1667.e8 (2018).
26. E. Kim *et al.*, Mouse sperm lacking ADAM1b/ADAM2 fertilin can fuse with the egg plasma membrane and effect fertilization. *J. Biol. Chem.* **281**, 5634–5639 (2006).
27. A. K. Lakkaraju *et al.*, Palmitoylated calnexin is a key component of the ribosome–translocon complex. *EMBO J.* **31**, 1823–1835 (2012).
28. M. S. Rana *et al.*, Fatty acyl recognition and transfer by an integral membrane *S* -acyltransferase. *Science* **359**, eaao6326 (2018).
29. J. Abramson *et al.*, Accurate structure prediction of biomolecular interactions with AlphaFold 3. *Nature* **630**, 493–500 (2024).
30. X. Huang *et al.*, S-acylation of p62 promotes p62 droplet recruitment into autophagosomes in mammalian autophagy. *Mol. Cell* **83**, 3485–3501.e11 (2023).
31. J. Gao, W. Li, Z. Zhang, W. Gao, E. Kong, Proteome-wide identification of palmitoylated proteins in mouse testis. *Reproduct. Sci.* **29**, 2299–2309 (2022).
32. J. Wan, A. F. Roth, A. O. Bailey, N. G. Davis, Palmitoylated proteins: Purification and identification. *Nat. Protoc.* **2**, 1573–1584 (2007).
33. S. Bao *et al.*, Male mice that do not express group VIA phospholipase A2 produce spermatozoa with impaired motility and have greatly reduced fertility. *J. Biol. Chem.* **279**, 38194–38200 (2004).
34. C. Meyer *et al.*, μ1A-adaptin-deficient mice: Lethality, loss of AP-1 binding and rerouting of mannose 6-phosphate receptors. *EMBO J.* **19**, 2193–2203 (2000).
35. Y. Wu *et al.*, Retinoic acid induced protein 14 (Rai14) is dispensable for mouse spermatogenesis. *PeerJ* **9**, e10847 (2021).
36. K. Shimada *et al.*, TSKS localizes to nuage in spermatids and regulates cytoplasmic elimination during spermiation. *Proc. Natl. Acad. Sci. U.S.A.* **120**, e2221762120 (2023).
37. C. Salaun, C. Locatelli, F. Zmuda, J. Cabrera González, L. H. Chamberlain, Accessory proteins of the zDHHC family of S-acylation enzymes. *J. Cell Sci.* **133**, jcs251819 (2020).
38. J. T. Swarthout *et al.*, DHHC9 and GCP16 constitute a human protein fatty acyltransferase with specificity for H- and N-Ras. *J. Biol. Chem.* **280**, 31141–31148 (2005).
39. G. Drewes, A. Ebneth, U. Preuss, E.-M. Mandelkow, E. Mandelkow, MARK, a novel family of protein kinases that phosphorylate microtubule-associated proteins and trigger microtubule disruption. *Cell* **89**, 297–308 (1997).
40. Y. Wu, E. E. Griffin, Regulation of cell polarity by PAR-1/MARK kinase. *Curr. Top. Dev. Biol.* **123**, 365–397 (2017).
41. D. Cohen, P. J. Brennwald, E. Rodriguez-Boulan, A. Müsch, Mammalian PAR-1 determines epithelial lumen polarity by organizing the microtubule cytoskeleton. *J. Cell Biol.* **164**, 717–727 (2004).
42. F. Lázaro-Diéguez *et al.*, Par1b links lumen polarity with LGN–NuMA positioning for distinct epithelial cell division phenotypes. *J. Cell Biol.* **203**, 251–264 (2013).
43. I. Zulkipli *et al.*, Spindle rotation in human cells is reliant on a MARK2-mediated equatorial spindle-centering mechanism. *J. Cell Biol.* **217**, 3057–3070 (2018).
44. T. Sapir *et al.*, Accurate balance of the polarity kinase MARK2/Par-1 is required for proper cortical neuronal migration. *J. Neurosci.* **28**, 5710–5720 (2008).
45. J. A. McDonald, Canonical and noncanonical roles of Par-1/MARK kinases in cell migration. *Int. Rev. Cell Mol. Biol.* **312**, 169–199 (2014).
46. A. M. Pasapera *et al.*, MARK2 regulates directed cell migration through modulation of myosin II contractility and focal adhesion organization. *Curr. Biol.* **32**, 2704–2718.e6 (2022).
47. E. I. Tang, C. Y. Cheng, MARK2 and MARK4 regulate sertoli cell BTB dynamics through microtubule and actin cytoskeletons. *Endocrinology* **163**, bqac130 (2022).
48. S. Bessone *et al.*, EMK protein kinase–null mice: Dwarfism and hypofertility associated with alterations in the somatotrope and prolactin pathways. *Dev. Biol.* **214**, 87–101 (1999).
49. C. Sun *et al.*, Inactivation of MARK4, an AMP-activated protein kinase (AMPK)-related kinase, leads to insulin hypersensitivity and resistance to diet-induced obesity. *J. Biol. Chem.* **287**, 38305–38315 (2012).
50. E. I. Tang *et al.*, Microtubule affinity-regulating kinase 4 (MARK4) is a component of the ectoplasmic specialization in the rat testis. *Spermatogenesis* **2**, 117–126 (2012).
51. M.-J. Sandí *et al.*, MARK3-mediated phosphorylation of ARHGEF2 couples microtubules to the actin cytoskeleton to establish cell polarity. *Sci. Signal* **10**, eaan3286 (2017).
52. A. F. O'Donnell, M. C. Schmidt, AMPK-mediated regulation of alpha-arrestins and protein trafficking. *Int. J. Mol. Sci.* **20**, 515 (2019).
53. K. Zbieralski, D. Wawrzycka, α-Arrestins and Their Functions: From Yeast to Human Health. *Int. J. Mol. Sci.* **23**, 4988 (2022).
54. Y. Shang *et al.*, Essential role for SUN5 in anchoring sperm head to the tail. *eLife* **6**, e28199 (2017).
55. T.-H. Lai *et al.*, SEPT12–NDC1 Complexes Are Required for Mammalian Spermiogenesis. *Int. J. Mol. Sci.* **17**, 1911 (2016).
56. Y. Kaneda *et al.*, FBXO24 deletion causes abnormal accumulation of membraneless electron-dense granules in sperm flagella and male infertility. *eLife* **13**, RP92794 (2024).
57. Y. Ho, K. Wigglesworth, J. J. Eppig, R. M. Schultz, Preimplantation development of mouse embryos in KSOM: Augmentation by amino acids and analysis of gene expression. *Mol. Reprod. Dev.* **41**, 232–238 (1995).
58. Y. Kaneda, H. Miyata, K. Shimada, S. Oura, M. Ikawa, Testis-specific proteins, TSNAXIP1 and 1700010I14RIK, are important for sperm motility and male fertility in mice. *Andrology* **11**, 799–807 (2023).